Functional Nanoparticles

DOI: 10.1002/anie.201209903

Core–Shell Noble-Metal@Metal-Organic-Framework Nanoparticles with Highly Selective Sensing Property**

Liangcan He, Yong Liu, Jingzhu Liu, Yansong Xiong, Jianzhong Zheng, Yaling Liu, and Zhiyong Tang**

Noble-metal nanoparticles (NPs) (such as Au, Ag, Pd, and Pt) have been the subject of intense research because their unique physiochemical properties are different from those of their bulk counterparts[1] and various applications are anticipated in sensing,[2] imaging,[3] cancer therapy,[4] optical data storage,[5] and catalysis.[6] However, it is well known that free noble-metal NPs have high surface energies and tend to aggregate and fuse; as a result the intriguing properties observed for the NPs disappear and difficulties arise for long-term storage, processing, and applications. Therefore, great efforts have been devoted to develop novel strategies to stabilize NPs,[7] and the most common approach is to coat noble-metal NPs with either organic or inorganic shells. These shells not only endow NPs with high stability but also offer them additional functionalities. As an example, in addition to good stability and biocompatibility, the mesoporous silica shells that are currently broadly used have high surface area and tunable pore size and volume, which can accommodate analytes and drug molecules.[7,8] Unfortunately, the amorphous structure of silica and its own characteristics determine that it may be used only as a carrier, stabilizer, and ligand linker. In order to break through the limitations and develop a wide range of applications, it is necessary to search for new types of shell materials that not only have properties similar to those of porous silica but also impart new functionalities.

In addition to high specific surface area and tunable pore size and volume, metal–organic frameworks (MOFs) have many exciting characteristics including structural adaptivity and flexibility, ordered crystalline pores, and multiple coordination sites, and offer various functions such as chemical separation,[9] gas storage,[10] drug delivery,[11] sensing,[12] and catalysis,[13] which originate from the limitless choice of building blocks.[14] Recently, MOFs have been used as functional materials to fabricate nanostructures with noble-metal NPs by either embedding NPs in the MOF matrices or encapsulating NPs within the MOF layers.[15] Nevertheless, effective control over the dispersibility of NPs within MOFs as well as the morphology and size of the composite products still presents significant challenges. For example, to our knowledge, there are few reports about the construction of well-defined core–shell noble-metal@MOF NPs,[15f,g] and none on the successful synthesis of core–shell noble-metal@-MOF NPs with a single metal NP core coated with a uniform MOF shell. Herein, we report a facile one-pot method to prepare core–shell Au@MOF-5 ($Zn_4O(BDC)_3$, BDC = 1,4-benzenedicarboxylate) NPs with uniform shape and tunable size, in which the single Au NP core is coated with a uniform MOF-5 shell. Impressively, the core–shell Au@MOF-5 NPs with a specific shell thickness are highly selective sensors of CO_2 in gas mixtures.

Different from the conventional two-step method to synthesize NP@MOF composites by adding the presynthesized NPs into the MOF precursors, we prepared the core–shell Au@MOF-5 NPs by directly mixing both the Au and MOF precursors ($HAuCl_4$, $Zn(NO_3)_2{\cdot}6H_2O$, and H_2BDC) in the reaction solution containing *N*,*N*-dimethylformamide (DMF), polyvinylpyrrolidone (PVP), and ethanol (see Part S1 in the Supporting Information). By controlling the reaction conditions, the formation rates of Au NPs and MOF-5 in the mixture solution could be adjusted effectively. It was found that at 140 °C $HAuCl_4$ was first reduced to Au NPs by DMF within a very short time (Figure S1a).[16] Subsequently, MOF-5 formed and spontaneously grew on the surface of the PVP-capped Au NPs, so that uniform PVP-stabilized core–shell Au@MOF-5 NPs were produced (Figure S1b–d). Finally, the PVP stabilizer and DMF were removed from the core–shell NPs by rinsing with DMF and $CHCl_3$ several times. The core–shell NPs were dried under vacuum at 120 °C for 36 h before further characterization and performance measurements (see Part S1 in the Supporting Information). It should be noted that DMF, PVP, and ethanol are indispensable to the preparation of the core–shell Au@MOF-5 NPs. DMF is the solvent for the H_2BDC solution and directly determines whether MOF-5 can be produced; meanwhile, it is also the reducing agent for the synthesis of Au NPs within the core–shell structures.[16] PVP acts as the stabilizer of Au NPs.[15g,16b] When no PVP was added to the reaction solution, the produced Au NPs readily aggregated before the MOF-5 shell was synthesized, and no core–shell NPs like those shown in Figure 1 a–c were obtained (Figure S2). Ethanol is also vital for the formation of the core–shell NPs; its presence can

[*] L. He, Y. Liu, J. Liu, Y. Xiong, J. Zheng, Prof. Y. Liu, Prof. Z. Tang
National Center for Nanoscience and Technology
Beijing 100190 (P. R. China)
E-mail: liuyl@nanoctr.cn
zytang@nanoctr.cn

L. He, Y. Xiong
Department of Chemistry, Tsinghua University
Beijing 100084 (P. R. China)

[**] This work was supported financially by the National Natural Science Foundation for Distinguished Youth Scholars of China (21025310, Z.Y.T.), the National Natural Science Foundation of China (20901019, Y.L.L.; 20973047, Z.Y.T.; 91027011, Z.Y.T.), the National Research Fund for Fundamental Key Project (2009CB930401, Z.Y.T.), and the China-Korea Joint Research Project (2010DFA51700, Z.Y.T.).

Supporting information for this article is available on the WWW under http://dx.doi.org/10.1002/anie.201209903.

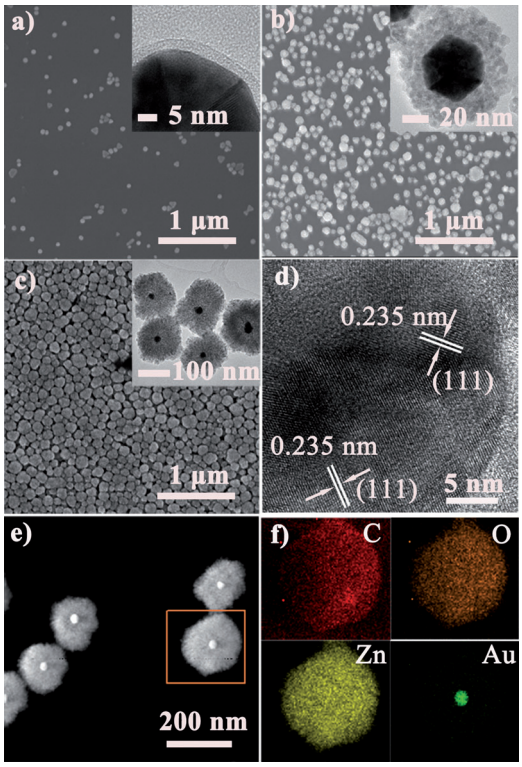

Figure 1. Scanning electron microscopy (SEM) and transmission electron microscopy (TEM) (inset) images of the core–shell Au@MOF-5 NPs with shell thicknesses of a) (3.2 ± 0.5) nm, b) (25.1 ± 4.1) nm, and c) (69.0 ± 12.4) nm. d) HRTEM image of a core–shell Au@MOF-5 NP. e) HAADF-STEM image of core–shell Au@MOF-5 NPs with a shell thickness of (69.0 ± 12.4) nm. f) EDX elemental mapping of the core–shell Au@MOF-5 NP marked in (e).

change the coordination environment of metal ions such that MOF-5 grows preferentially around the Au NPs instead of self-nucleating in solution (Figure S3).[17]

Figure 1 shows that all the NP products have well-defined core–shell structures with uniform size and shape (see also Figure S4 in the Supporting Information). Further statistics based on the products shown in Figure 1 a–c indicate that the shell thickness can be controlled from several nanometers ((3.2 ± 0.5) nm, Figure S5a) to several tens of nanometers ((69.0 ± 12.4) nm, Figure S5c), while the diameter of the Au NP cores varies from (54.0 ± 7.4) nm to (30.0 ± 7.0) nm (Figure S5), and correspondingly the size of the core–shell Au@MOF-5 NPs can be tuned from (60.7 ± 6.5) nm to (156.9 ± 19.8) nm, when the added amount of the Au precursors in the reaction solution is simply changed. Thanks to the rapid growth rate of the Au NP cores compared with the MOF-5 shells, the more Au precursors are added, the larger Au NP cores are produced, and correspondingly, the MOF-5 shells grown are thinner in the resulting core–shell NPs. Analysis of the cores by high-resolution transmission electron microscopy (HRTEM) imaging indicates that the spacing between two adjacent lattice planes is about 0.235 nm (Figure 1 d). This value is in agreement with the spacing of (111) planes of cubic Au, suggesting that the cores in the core–shell NPs are Au. Unfortunately, an atomic image of the shell is not possible by HRTEM imaging, and one plausible explanation is that the organic–inorganic MOFs are not stable to the illumination of high-energy electron beam.[15e] Nevertheless, powder X-ray diffraction (XRD) patterns further confirm that such core–shell NPs are composed of two components: face-centered-cubic Au (JCPDS card no. 001-1172) and cubic crystalline MOF-5 (Figure 2),[18] and no peak assigned to

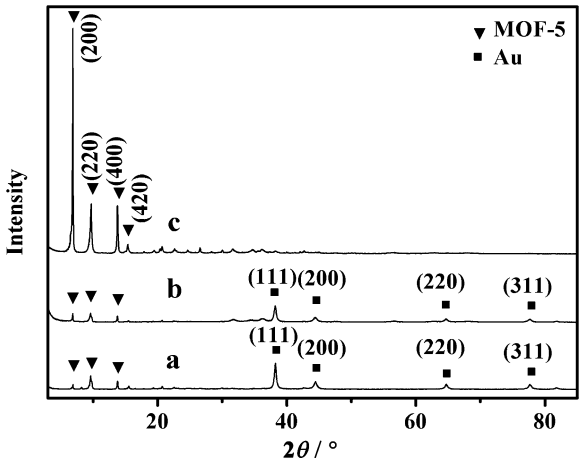

Figure 2. Powder XRD patterns of core–shell Au@MOF-5 NPs with shell thicknesses of a) (3.2 ± 0.5) nm, b) (25.1 ± 4.1) nm, and c) (69.0 ± 12.4) nm. Two series of peaks are assigned perfectly to the face-centered-cubic Au (marked with squares) and cubic crystalline MOF-5 (marked with triangles).[18]

other impurities is detected. Finally, the composition of the core–shell NPs is directly evident in high-angle annular dark-field scanning transmission electron microscopy (HAADF-STEM) imaging and energy-dispersive X-ray (EDX) elemental mapping (Figure 1 e,f). The HAADF-STEM image (Figure 1 e) clearly demonstrates that the produced NPs have a typical core–shell structure, and EDX elemental mapping further shows that the element Au is distributed only in the core and that the elements C, O, and Zn of MOF-5 are homogenously distributed throughout the whole NP (Figure 1 f), suggesting that a Au NP core is surrounded with a uniform MOF-5 shell.

The features of the MOF shells, especially the porosity, determine the properties of the core–shell NPs. All of the obtained core–shell Au@MOF-5 NPs were characterized by Brunauer–Emmett–Teller (BET) analysis. Figure 3 presents the corresponding N_2 adsorption–desorption isotherms of the core–shell Au@MOF-5 NPs with different shell thicknesses shown in Figure 1 a–c. The core–shell Au@MOF-5 NPs with shell thicknesses of (3.2 ± 0.5) nm and (25.1 ± 4.1) nm exhibit a typical type I N_2 isotherm (curve a and curve b, respectively, in Figure 3), characteristic of the micropores.[15g] In comparison, the core–shell Au@MOF-5 NPs with a shell thickness of (69.0 ± 12.4) nm show a type IV sorption isotherm with an H3 hysteresis loop (curve c in Figure 3), demonstrating the mesoporosity of the NPs.[19] The conversion from micropores to mesopores is also supported by pore size distribution measurements, in which the average size of the pores increases from 0.47 nm to 3.84 nm when the thickness of the

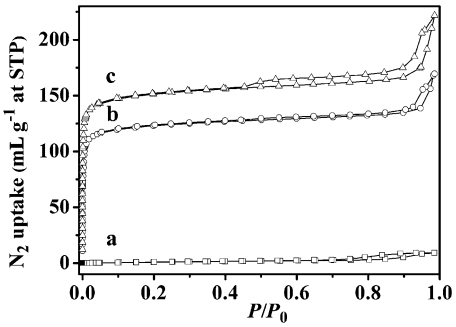

Figure 3. N_2 adsorption–desorption isotherms of the core–shell Au@MOF-5 NPs with shell thicknesses of a) (3.2 ± 0.5) nm, b) (25.1 ± 4.1) nm, and c) (69.0 ± 12.4) nm.

MOF-5 shells increases (Figure S6). The mesopores mainly originate from the voids between MOF aggregates in the thick shells, which is consistent with the TEM observation that the surface of the thick shells is much rougher than that of the thin shells (Figure 1 a–c and Figure S4).[20] Moreover, as the shell thickness increases, the corresponding surface area of the core–shell NPs increases from 7.0 $m^2 g^{-1}$ to 599.7 $m^2 g^{-1}$ owing to the decreasing contribution of nonporous Au NP cores to the mass of the core–shell NPs (Table S1).

The integration of MOF-5 and Au NPs into well-defined core–shell NPs might generate many new functionalities. For example, MOF-5 is known to be an attractive adsorbent for the separation of CO_2 from flue gas, because compared with N_2, O_2, CO, and other components of flue gas, CO_2 has higher polarizability and quadrupole moment, resulting in the stronger electrostatic attraction between the partially charged carbon atoms in CO_2 and the aromatic rings in MOF-5.[9a,10d,21] On the other hand, this dramatic amplification of the electromagnetic field surrounding Au NPs endows themselves many optical applications, for example, surface-enhanced Raman scattering (SERS) for highly sensitive detection. Therefore, core–shell Au@MOF-5 NPs can be expected to function as sensors for the selective detection of CO_2 since they take advantage of the selective adsorption property of the MOF-5 shell and the tremendous optical enhancement of the Au NP core.

The SERS performance of the core–shell Au@MOF-5 NPs with different shell thicknesses was investigated along with that of a couple of the contrast samples including bare Au NPs (Figure S7a) and pure MOF-5 spheres (Figure S7b), and the results are shown in Figure 4 a. It should be pointed out that in order to avoid the possible influence of aggregation number and conformation, all the investigations were conducted on single NPs that were pre-positioned by SEM imaging (Figure S8). All the samples were put into a sealed flask that was filled with the mixture gas for 6 h before SERS measurement. Impressively, only the core–shell Au@MOF-5 NPs with a shell thickness of (3.2 ± 0.5) nm exhibit highly selective sensing toward CO_2 in the CO_2/N_2 gas mixture (trace 5 in Figure 4 a), whereas no Raman signals are observed for bare Au NPs ((60.5 ± 11.2) nm, Figure S7d), pure MOF-5 spheres, and even the core–shell Au@MOF-5 NPs with shell thicknesses of (25.1 ± 4.1) nm and (69.0 ± 12.4) nm (traces 1–4 in Figure 4 a, and Figure S9). This comparison demonstrates that selective detection of CO_2 is realized only by the combination of Au NP and MOF-5 in the specific core–shell nanostructure (Figure 1 a) and moreover, the shell thickness is a key factor in determining the test results.[22] It is well known that the electromagnetic enhancement of Au NPs is near field, mostly within a distance of less than 3 nm.[22,23] For the core–shell Au@MOF-5 NPs with a shell thickness of (3.2 ± 0.5) nm, the shell is thin enough, allowing not only selective capture of CO_2 molecules but also maximization of the detected SERS intensity. Thus, a characteristic Raman peak corresponding to the symmetric stretching vibration of CO_2 appears at 1395 cm^{-1} (trace 5 in Figure 4 a) and the SERS enhancement factor is 2.4×10^3 (see Part S3 in the Supporting Information).[23] For core–shell Au@MOF-5 NPs with a shell thickness of (69.0 ± 12.4) nm (trace 3 in Figure 4 a) or (25.1 ± 4.1) nm (trace 4 in Figure 4 a), the thick shells make the diffusion of CO_2 into the interface of the Au NP cores difficult, while the captured molecules far away from the Au NP cores could not contribute the SERS signal significantly.[24] In contrast, for

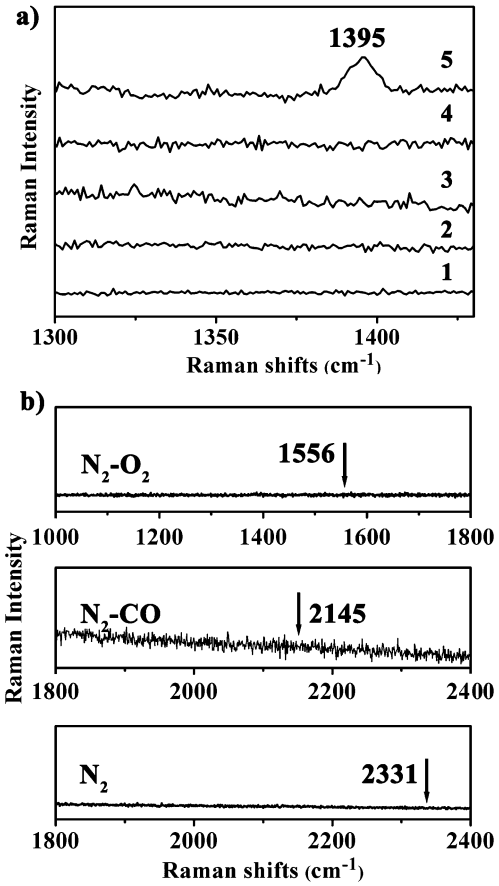

Figure 4. a) SERS spectra of single Au NPs (trace 1), single MOF-5 spheres (trace 2), and single core–shell Au@MOF-5 NPs with a shell thickness of $(69.0\pm12.4$ nm) (trace 3), 25.1 ± 4.1 nm (trace 4), and (3.2 ± 0.5) nm (trace 5) toward CO_2 in the CO_2/N_2 gas mixture (the ratio is 1:5 for CO_2 vs. N_2) at room temperature. b) SERS spectra of single core–shell Au@MOF-5 NP with a shell thickness of (3.2 ± 0.5) nm toward N_2, CO, and O_2. The arrows point to the characteristic SERS peak positions of N_2, CO, and O_2.

bare Au NPs, though diffusion into the interface is easy, selective enrichment of CO_2 nearby the Au NPs is absent (trace 1 in Figure 4a). Accordingly, both cases did not result in high response to CO_2. Furthermore, for pure MOF-5 spheres (trace 2 in Figure 4a), the lack of Raman signature is understood since the dramatic amplification effect of Au NPs does not exist.

Lastly, we found that the core–shell Au@MOF-5 NPs with a shell thickness of (3.2 ± 0.5) nm have no SERS activity toward other possible interferents such as N_2, CO, and O_2 (Figure 4b and Figure S10, the specific frequency vibration signals for gas-phase N_2, O_2, and CO are 2331 cm^{-1}, 1556 cm^{-1}, and 2145 cm^{-1}, respectively).[23] Evidently, the highly selective sensing property should originate from the specific adsorption capability of the MOF-5 shell toward CO_2 molecules.

In summary, we have successfully prepared core–shell Au@MOF-5 NPs in which a single Au NP core is coated with a uniform MOF-5 shell. Notably, this is the first example of core–shell noble-metal@MOF NPs with a single metal NP core. Moreover, the one-pot synthesis method used in the work is a general technique for the preparation of different types of core–shell noble-metal@MOF NPs, for example, Au@ZIF-8 NPs, Au@IRMOF-3 NPs, and Ag@MOF-5 NPs (Figure S11). Compared with bare Au NPs and pure MOF-5 spheres, the core–shell Au@MOF-5 NPs with a shell thickness of (3.2 ± 0.5) nm show unique SERS activity toward CO_2 in gas mixtures. Such sensitive SERS detection can be easily applied to other analytes including dimethylformamide and ethanol by using the core–shell Au@MOF-5 NPs and core–shell Au@ZIF-8 NPs, respectively (Figure S12). Considering the excellent properties and broad applications of both noble-metal NPs and MOFs, we anticipate that this new type of core–shell nanostructure will find use in many fields such as catalysis, sensors, and drug delivery.[15f,g]

Received: December 11, 2012
Published online: February 18, 2013

Keywords: core–shell nanoparticles · gold · metal–organic frameworks · sensors

[1] a) S. Liu, Z. Tang, *J. Mater. Chem.* **2010**, *20*, 24 – 35; b) D. Astruc, F. Lu, J. R. Aranzaes, *Angew. Chem.* **2005**, *117*, 8062 – 8083; *Angew. Chem. Int. Ed.* **2005**, *44*, 7852 – 7872; c) N. Tian, Z. Zhou, S. Sun, Y. Ding, Z. Wang, *Science* **2007**, *316*, 732 – 735.

[2] a) J. N. Anker, W. P. Hall, O. Lyandres, N. C. Shah, J. Zhao, R. P. Van Duyne, *Nat. Mater.* **2008**, *7*, 442 – 453; b) C. Gao, Z. Lu, Y. Liu, Q. Zhang, M. Chi, Q. Cheng, Y. Yin, *Angew. Chem.* **2012**, *124*, 5727 – 5731; *Angew. Chem. Int. Ed.* **2012**, *51*, 5629 – 5633.

[3] a) N. J. Durr, T. Larson, D. K. Smith, B. A. Korgel, K. Sokolov, A. Ben-Yakar, *Nano Lett.* **2007**, *7*, 941 – 945; b) C. J. Murphy, A. M. Gole, S. E. Hunyadi, J. W. Stone, P. N. Sisco, A. Alkilany, B. E. Kinard, P. Hankins, *Chem. Commun.* **2008**, 544 – 557.

[4] X. Huang, I. H. El-Sayed, W. Qian, M. A. El-Sayed, *Nano Lett.* **2007**, *7*, 1591 – 1597.

[5] a) J. W. M. Chon, C. Bullen, P. Zijlstra, M. Gu, *Adv. Funct. Mater.* **2007**, *17*, 875 – 880; b) P. Zijlstra, J. W. M. Chon, M. Gu, *Nature* **2009**, *459*, 410 – 413.

[6] a) D. Astruc, *Nanoparticles and Catalysis*, *Vol. 2*, Wiley-VCH, Weinheim, **2008**, pp. 1 – 640; b) C. Burda, X. Chen, R. Narayanan, M. A. El-Sayed, *Chem. Rev.* **2005**, *105*, 1025 – 1102.

[7] a) W.-T. Chen, T.-T. Yang, Y.-J. Hsu, *Chem. Mater.* **2008**, *20*, 7204 – 7206; b) C. Gao, Q. Zhang, Z. Lu, Y. Yin, *J. Am. Chem. Soc.* **2011**, *133*, 19706 – 19709.

[8] a) J. Liu, S. Qiao, S. B. Hartono, G. Lu, *Angew. Chem.* **2010**, *122*, 5101 – 5105; *Angew. Chem. Int. Ed.* **2010**, *49*, 4981 – 4985; b) I. I. Slowing, B. G. Trewyn, V. S. Y. Lin, *J. Am. Chem. Soc.* **2007**, *129*, 8845 – 8849; c) M. Vallet-Regí, F. Balas, D. Arcos, *Angew. Chem.* **2007**, *119*, 7692 – 7703; *Angew. Chem. Int. Ed.* **2007**, *46*, 7548 – 7558; d) M. Vallet-Regi, A. Rámila, R. P. del Real, J. Pérez-Pariente, *Chem. Mater.* **2001**, *13*, 308 – 311.

[9] a) J. Li, J. Sculley, H. Zhou, *Chem. Rev.* **2012**, *112*, 869 – 932; b) J. S. Seo, D. Whang, H. Lee, S. I. Jun, J. Oh, Y. J. Jeon, K. Kim, *Nature* **2000**, *404*, 982 – 986; c) S. Xiang, Z. Zhang, C. Zhao, K. Hong, X. Zhao, D. Ding, M. Xie, C. Wu, M. C. Das, R. Gill, K. M. Thomas, B. Chen, *Nat. Commun.* **2011**, *2*, 204.

[10] a) Y.-S. Bae, R. Q. Snurr, *Angew. Chem.* **2011**, *123*, 11790 – 11801; *Angew. Chem. Int. Ed.* **2011**, *50*, 11586 – 11596; b) N. L. Rosi, J. Eckert, M. Eddaoudi, D. T. Vodak, J. Kim, M. O'Keeffe, O. M. Yaghi, *Science* **2003**, *300*, 1127 – 1129; c) M. P. Suh, H. J. Park, T. K. Prasad, D.-W. Lim, *Chem. Rev.* **2012**, *112*, 782 – 835; d) K. Sumida, D. L. Rogow, J. A. Mason, T. M. McDonald, E. D. Bloch, Z. R. Herm, T.-H. Bae, J. R. Long, *Chem. Rev.* **2012**, *112*, 724 – 781.

[11] a) P. Horcajada, T. Chalati, C. Serre, B. Gillet, C. Sebrie, T. Baati, J. F. Eubank, D. Heurtaux, P. Clayette, C. Kreuz, J.-S. Chang, Y. K. Hwang, V. Marsaud, P.-N. Bories, L. Cynober, S. Gil, G. Ferey, P. Couvreur, R. Gref, *Nat. Mater.* **2010**, *9*, 172 – 178; b) P. Horcajada, C. Serre, G. Maurin, N. A. Ramsahye, F. Balas, M. Vallet-Regí, M. Sebban, F. Taulelle, G. Férey, *J. Am. Chem. Soc.* **2008**, *130*, 6774 – 6780; c) J. Della Rocca, D. Liu, W. Lin, *Acc. Chem. Res.* **2011**, *44*, 957 – 968.

[12] L. E. Kreno, K. Leong, O. K. Farha, M. Allendorf, R. P. Van Duyne, J. T. Hupp, *Chem. Rev.* **2012**, *112*, 1105 – 1125.

[13] a) J. Lee, O. K. Farha, J. Roberts, K. A. Scheidt, S. T. Nguyen, J. T. Hupp, *Chem. Soc. Rev.* **2009**, *38*, 1450 – 1459; b) M. Yoon, R. Srirambalaji, K. Kim, *Chem. Rev.* **2012**, *112*, 1196 – 1231.

[14] a) C. Janiak, J. K. Vieth, *New J. Chem.* **2010**, *34*, 2366 – 2388; b) J. R. Long, O. M. Yaghi, *Chem. Soc. Rev.* **2009**, *38*, 1213 – 1214.

[15] a) S. Hermes, M.-K. Schröter, R. Schmid, L. Khodeir, M. Muhler, A. Tissler, R. W. Fischer, R. A. Fischer, *Angew. Chem.* **2005**, *117*, 6394 – 6397; *Angew. Chem. Int. Ed.* **2005**, *44*, 6237 – 6241; b) H. Jiang, B. Liu, T. Akita, M. Haruta, H. Sakurai, Q. Xu, *J. Am. Chem. Soc.* **2009**, *131*, 11302 – 11303; c) M. Meilikhov, K. Yusenko, D. Esken, S. Turner, G. Van Tendeloo, R. A. Fischer, *Eur. J. Inorg. Chem.* **2010**, 3701 – 3714; d) C. Zlotea, R. Campesi, F. Cuevas, E. Leroy, P. Dibandjo, C. Volkringer, T. Loiseau, G. Férey, M. Latroche, *J. Am. Chem. Soc.* **2010**, *132*, 2991 – 2997; e) R. J. T. Houk, B. W. Jacobs, F. E. Gabaly, N. N. Chang, A. A. Talin, D. D. Graham, S. D. House, I. M. Robertson, M. D. Allendorf, *Nano Lett.* **2009**, *9*, 3413 – 3418; f) D. Buso, K. M. Nairn, M. Gimona, A. J. Hill, P. Falcaro, *Chem. Mater.* **2011**, *23*, 929 – 934; g) G. Lu, S. Li, Z. Guo, O. K. Farha, B. G. Hauser, X. Qi, Y. Wang, X. Wang, S. Han, X. Liu, J. S. DuChene, H. Zhang, Q. Zhang, X. Chen, J. Ma, S. C. J. Loo, W. D. Wei, Y. Yang, J. T. Hupp, F. Huo, *Nat. Chem.* **2012**, *4*, 310 – 316; h) K. Sugikawa, Y. Furukawa, K. Sada, *Chem. Mater.* **2011**, *23*, 3132 – 3134; i) T. Tsuruoka, H. Kawasaki, H. Nawafune, K. Akamatsu, *ACS Appl. Mater. Interfaces* **2011**, *3*, 3788 – 3791; j) P. Falcaro, A. J. Hill, K. M. Nairn, J. Jasieniak, J. I. Mardel, T. J. Bastow, S. C. Mayo, M. Gimona, D. Gomez, H. J. Whitfield, R. Riccò, A. Patelli, B. Marmiroli, H. Amenitsch, T. Colson, L. Villanova, D. Buso, *Nat. Commun.* **2011**, *2*, 237.

[16] a) I. Pastoriza-Santos, L. M. Liz-Marzán, *Adv. Funct. Mater.* **2009**, *19*, 679 – 688; b) L. Rodríguez-Lorenzo, R. de La Rica,

R. A. Álvarez-Puebla, L. M. Liz-Marzán, M. M. Stevens, *Nat. Mater.* **2012**, *11*, 604 – 607.
[17] a) Y.-S. Bae, A. M. Spokoyny, O. K. Farha, R. Q. Snurr, J. T. Hupp, C. A. Mirkin, *Chem. Commun.* **2010**, *46*, 3478 – 3480; b) S. K. Batabyal, C. Basu, A. R. Das, G. S. Sanyal, *Cryst. Growth Des.* **2004**, *4*, 509 – 511.
[18] H. Li, M. Eddaoudi, M. O'Keeffe, O. M. Yaghi, *Nature* **1999**, *402*, 276 – 279.
[19] Y. Zhao, J. Zhang, B. Han, J. Song, J. Li, Q. Wang, *Angew. Chem.* **2011**, *123*, 662 – 665; *Angew. Chem. Int. Ed.* **2011**, *50*, 636 – 639.
[20] O. K. Farha, A. M. Spokoyny, K. L. Mulfort, S. Galli, J. T. Hupp, C. A. Mirkin, *Small* **2009**, *5*, 1727 – 1731.
[21] a) K. S. Walton, A. R. Millward, D. Dubbeldam, H. Frost, J. J. Low, O. M. Yaghi, R. Q. Snurr, *J. Am. Chem. Soc.* **2008**, *130*, 406 – 407; b) Z. Zhao, Z. Li, Y. S. Lin, *Ind. Eng. Chem. Res.* **2009**, *48*, 10015 – 10020; c) D. Saha, Z. Bao, F. Jia, S. Deng, *Environ. Sci. Technol.* **2010**, *44*, 1820 – 1826; d) A. Martín-Calvo, E. García-Pérez, J. Manuel Castillo, S. Calero, *Phys. Chem. Chem. Phys.* **2008**, *10*, 7085 – 7091.
[22] J. Li, Y. Huang, Y. Ding, Z. Yang, S. Li, X. Zhou, F. Fan, W. Zhang, Z. Zhou, D. Wu, B. Ren, Z. Wang, Z. Tian, *Nature* **2010**, *464*, 392 – 395.
[23] S. A. Tedder, J. L. Wheeler, A. D. Cutler, P. M. Danehy, *Appl. Opt.* **2010**, *49*, 1305 – 1313.
[24] Q. Ye, J. Fang, L. Sun, *J. Phys. Chem. B* **1997**, *101*, 8221 – 8224.

